Statistics of polarization and Stokes parameters of stochastic waves

M. J. Hole, P. A. Robinson, and Iver H. Cairns
School of Physics, University of Sydney, Sydney, New South Wales 2006, Australia
(Received 17 March 2004; published 30 September 2004)

Several theories now exist to describe the probability distribution functions (PDFs) for the electric field strength, intensity, and power of signals. In this work, a model is developed for the PDFs of the polarization properties of the superposition of multiple transverse wave populations. The polarization of each transverse wave population is described by a polarization ellipse with fixed axial ratio and polarization angle, and PDFs for the field strength and phase. Wave populations are vectorially added, and expressions found for the Stokes parameters *I*, *U*, *Q*, and *V*, as well as the degrees of linear and circular polarization, and integral expressions for their statistics. In this work, lognormal distributions are chosen for the electric field, corresponding to stochastic growth, and polarization PDFs are numerically calculated for the superposition of orthonormal mode populations, which might represent the natural modes emitted by a source. Examples are provided of the superposition of linear, circular, and elliptically polarized wave populations in cases where the component field strength PDFs are the same, and where one field strength PDF is dominant.

DOI: 10.1103/PhysRevE.70.036619 PACS number(s): 42.25.Ja, 42.25.Dd, 52.35.−g, 02.50.Cw

I. INTRODUCTION

A range of theories now exist to describe wave field statistics in inhomogeneous plasmas, including self organized criticality (SOC) [1], scattering [2], turbulence [3], and stochastic growth theory (SGT) [4]. Physically, the various theories are differentiated by varying degrees of interaction between the waves, particles, and background plasma. These have the common feature of predicting probability distribution functions (PDFs) for the electric field strength. In this work a stochastic model for the measurable Stokes parameters *I*, *U*, *Q*, and *V* is produced from the vector addition of multiple wave populations. Each wave is assumed to be transverse with the same angular frequency ω and wave vector $\mathbf{k}$ [5,6], but random phases and amplitudes. The Stokes parameter *I* describes the intensity, $r_l=(\sqrt{U^2+Q^2})/I$ is the degree of linear polarization, and $v=V/I$ is the degree of circular polarization. Together, the set *I*, *U*, *Q*, *V*, (or *I*, *U*, r_l, v) fully describes the polarization of transverse waves. The motivations for developing such a model are to extend stochastic theories beyond electric field intensity predictions, and to obtain predictions for the PDFs of the measurable Stokes parameters for a model of superposed waves from multiple sources.

The problem is formulated in terms of the superposition of an arbitrary number of wave populations. Analytic expressions are then developed for the superposition of two modes with fixed but arbitrary axial ratios and polarization angles, and probability distribution functions for the field strength and phase. We focus on predictions for the superposition of two orthonormal modes, which is also a convenient (and natural) basis for treating emission from a source, such as a plasma. Here, we do not address the physics of the plasma source, nor do we consider mode conversion and propagation effects. Rather, we answer the more fundamental question of how to determine the polarization statistics of the superposition of two or more specified wave populations. This work differs from the body of literature that has developed to describe the statistics of unpolarized [7] and partially and fully polarized light [8–10] in that the PDFs of the component electric fields are arbitrary (here, only results for a lognormal distribution are presented), and that each wave population can be decomposed into an orthonormal pair of modes with fixed polarization angles and axial ratios.

Many phenomenological applications of the theory exist, in which the polarization of wave emission is either measured or measurable. Examples include waves in the Earth's foreshock [11–13], polar cap [14], and magnetosheath [15], type III solar radio bursts [16], and thermal noise in the solar wind [12], all of which can be described by SGT. Another possibility is the analysis and interpretation of polarity-resolved pulsar data (e.g., Vela [17]). Non-SGT examples include solar flare intensities, which obey a power-law distribution, consistent with self-organized criticality [18], and cyclotron maser emission in the *O* and *X* modes on auroral field lines, leading to polarized auroral kilometric radiation [19]. Possible analogs also exist in laboratory plasmas, where SOC has been invoked to describe properties of Langmuir probe measurements of plasma edge electrostatic fluctuations [20].

This paper is organized as follows. In Sec. II, theories for stochastic growth are briefly described, a stochastic description for the Stokes parameters is developed, and differences between this model and those of earlier stochastic models for the Stokes parameters explained in detail. Section III analyzes the superposition of two wave populations. Integral expressions for the PDFs of the Stokes parameters are derived, analyzed, and the numerical integration technique explained. In Sec. IV predictions for the PDFs are computed for a range of polarizations and field strength distributions. Finally, Sec. V outlines future work and contains concluding remarks.

II. STOCHASTIC ANALYSIS OF POLARIZATION PARAMETERS

Each of the theories mentioned in Sec. I predicts different PDFs for the wave electric field *E*. Self-organized criticality

[1], in which the wave-plasma system is driven away from dynamical equilibrium by input of free energy, but relaxes back via cascades triggered by the local onset of a instability at some threshold, predicts power-law distributions [21]. Scattering by density irregularities yields Gaussian intensity distributions [2], with intensity $I \propto E^2$. Power-law distributions are expected in strong turbulence; they become Gaussian in very strong turbulence [22]. Finally, stochastic growth theory [4], which we use as an example in Sec. IV, predicts lognormal statistics, with

$$P(\ln \tilde{E}) = \frac{1}{\sqrt{2\pi\sigma}} \exp\left(- \frac{(\ln \tilde{E} - \mu)^2}{2\sigma} \right). \tag{1}$$

where $\tilde{E} = E/E_0$ is a normalized electric field strength, E_0 is the reference field, and μ and σ are the mean and standard deviation in $\ln \tilde{E}$, where ln is the natural logarithm. For notational simplicity we hereafter set $E_0 = 1$ V/m, such that $\tilde{E}$ is a dimensionless quantity with value taking the magnitude of the electric field (measured in V/m), and drop the tilde on all normalized quantities.

A. Vector superposition model for polarization statistics

Our analysis of the polarization statistics of the vector superposition of two or more wave populations builds on earlier work by Cairns *et al.* [23], in which a vector addition model was developed for the intensity. In their work two populations of transverse electric field vectors with random strengths E_1 and E_2 and with random phase angle between them were convolved to describe the superposition of two signals. We generalize their analysis to consider the polarization of the superposition of multiple wave populations, each written in the axial formulation.

In the axial-ratio formulation an arbitrary transverse electric field vector can always be written

$$\mathbf{E} = \frac{E e^{i(\Phi - \omega t)}}{\sqrt{\gamma^2 + \delta^2}} (\gamma \mathbf{e}_x + \delta \mathbf{e}_y), \tag{2}$$

where γ and δ are arbitrary complex coefficients, $\mathbf{e}_x$ and $\mathbf{e}_y$ are orthonormal coordinates, Φ is a phase, and $\mathbf{k} = \mathbf{e}_x \times \mathbf{e}_y$ is the direction of wave propagation. It can be shown [5] that the unit vectors $(\mathbf{e}_x, \mathbf{e}_y)$ can always be rotated through an angle ϕ, such that the electric field can be rewritten

$$\mathbf{E} = \frac{E e^{i(\Phi - \omega t)}}{\sqrt{1 + T^2}} (T \mathbf{e}_t + i \mathbf{e}_a), \tag{3}$$

in terms of new unit vectors $(\mathbf{e}_t, \mathbf{e}_a)$, where the axial ratio T is real. As time advances, the real projections of Eq. (3) trace out an ellipse with axes along $\mathbf{e}_t$ and $\mathbf{e}_a$ and phase Φ. Figure 1 shows the coordinate geometry and the trajectory of the electric field vector tip for a wave with $T > 0$, and negative phase. As time advances the wave propagates into the page, while the wave vector rotates in a clockwise direction, and is said to be right-hand (RH) elliptically polarized. In this work we suppose that the i'th wave population has fixed axial ratio T_i and polarization angle ϕ_i, but random field strengths E_i and phase ϕ_i with PDFs $P(E_i)$ and $P(\Phi_i)$, respectively.

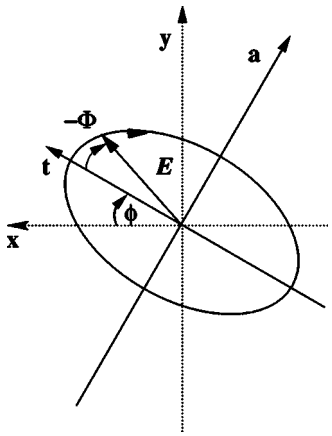

FIG. 1. The rotation of an arbitrary transverse wave vector through angle ϕ can always be written as a polarization ellipse with E the peak field strength, and Φ the phase. The wave propagates in the $\mathbf{k} = \mathbf{e}_x \times \mathbf{e}_y = \mathbf{e}_t \times \mathbf{e}_a$ direction, into the page. The mode drawn here rotates in a clockwise direction, and has a negative phase.

The Stokes parameters can be defined by [24]

$$I = \langle E_x E_x^* + E_y E_y^* \rangle, \tag{4}$$

$$Q = \langle E_x E_x^* - E_y E_y^* \rangle, \tag{5}$$

$$U = \langle E_x E_y^* + E_x^* E_y \rangle, \tag{6}$$

$$V = i \langle E_x E_y^* - E_x^* E_y \rangle, \tag{7}$$

where the angular brackets $\langle\ \rangle$ denote a time average over many cycles of the wave.

The Stokes parameters satisfy

$$I^2 = Q^2 + U^2 + V^2. \tag{8}$$

Using the electric field representation of Eq. (3), the Stokes parameters are

$$I = E^2, \tag{9}$$

$$Q = E^2 \left(\frac{T^2 - 1}{T^2 + 1} \right) \cos 2\phi, \tag{10}$$

$$U = E^2 \left(\frac{T^2 - 1}{T^2 + 1} \right) \sin 2\phi, \tag{11}$$

$$V = E^2 \left(\frac{2T}{T^2 + 1} \right). \tag{12}$$

For a single wave population with intensity distribution $P(E^2)$ the PDF of the Stokes parameters can be immediately computed by a change of variable, giving

$$P(I) = P(E^2), \tag{13}$$

$$P(Q) = P(E^2) \Big/ \left| \frac{\partial Q}{\partial E^2} \right| \tag{14}$$

$$= P(E^2) \left| \left(\frac{T^2+1}{T^2-1} \right) \sec 2\phi \right|, \tag{15}$$

$$P(U) = P(E^2) \Big/ \left| \frac{\partial Q}{\partial E^2} \right| \tag{16}$$

$$= P(E^2) \left| \left(\frac{T^2+1}{T^2-1} \right) \csc 2\phi \right|, \tag{17}$$

$$P(V) = P(E^2) \Big/ \left| \frac{\partial V}{\partial E^2} \right| = P(E^2) \left| \frac{T^2+1}{2T} \right|. \tag{18}$$

The PDF of the Stokes parameters of the sum of two or more wave populations of the same frequency, each with fixed and independent axial ratio T_i and polarization angle ϕ_i, but random field strength and phase differences with PDFs $P(E_i^2)$ and $P(\Phi_i - \Phi_j)$, respectively, can found by a change of variable, followed by integration over the component field strength distributions and all but one of the phase differences. Using S as a label for I, U, Q, or V we have

$$P(S, \Phi_3 - \Phi_1, \ldots, \Phi_n - \Phi_1, E_1^2, \ldots, E_n^2) \times \left| \frac{\partial(S, \Phi_3 - \Phi_1, \ldots, \Phi_n - \Phi_1, E_1^2, \ldots, E_n^2)}{\partial(\Phi_2 - \Phi_1, \ldots, \Phi_n - \Phi_1, E_1^2, \ldots, E_n^2)} \right|$$
$$= P(\Phi_2 - \Phi_1, \ldots, \Phi_n - \Phi_1, E_1^2, \ldots, E_n^2) \tag{19}$$

$$= \prod_{i=2}^{n} P(\Phi_i - \Phi_1) \prod_{j=1}^{n} P(E_j{}^2), \tag{20}$$

where independence of all $\Phi_i - \Phi_1$ and E_j has been assumed. Hence

$$P(S) = \int P(\Phi_2 - \Phi_1) \prod_{i=3}^{n} P(\Phi_i - \Phi_1) \prod_{j=1}^{n} P(E_j{}^2) \times \frac{d(\Phi_i - \Phi_1) dE_j{}^2}{\left| \frac{\partial(S, \Phi_3 - \Phi_1, \ldots, \Phi_n - \Phi_1, E_1^2, \ldots, E_n^2)}{\partial(\Phi_2 - \Phi_1, \ldots, \Phi_n - \Phi_1, E_1^2, \ldots, E_n^2)} \right|}. \tag{21}$$

The addition of any number of same frequency, copropagating, transverse electric fields can always be written in the form of Eq. (2). As such, using the transformation of Eq. (2) to Eq. (3) the superposed electric field vector will always trace out an ellipse, and so the set of PDFs $\{P(T), P(\Phi), P(E^2)\}$ of the superposed waves provides an equivalent and alternate stochastic description of the Stokes parameters $\{P(I), P(U), P(Q), P(V)\}$. In this work, we solve for PDFs of the Stokes parameters, as this provides direct comparison to measured quantities.

Finally, while the analysis in this section is applicable to arbitrary polarization, we predict the Stokes PDFs for the superposition of wave populations in pairs of orthonormal modes, being a natural and convenient basis. For transverse modes the orthonormality condition [5]

$$\mathbf{e}_{\mathrm{M2}}^{*}(\omega, \mathbf{k}) \cdot \mathbf{e}_{\mathrm{M1}}(\omega, \mathbf{k}) = 0 \tag{22}$$

must be satisfied, where $\mathbf{e}_{\mathrm{M1}}$ and $\mathbf{e}_{\mathrm{M2}}$ are the wave vectors of the modes of polarization. Using the axial ratio formulation [Eq. (3)] to represent the wave vectors $\mathbf{e}_{\mathrm{M1}}(\omega, \mathbf{k}) = \mathbf{E}_1 / E_1$ and $\mathbf{e}_{\mathrm{M2}}(\omega, \mathbf{k}) = \mathbf{E}_2 / E_2$, Eq. (22) is equivalent to $T_1 T_2 = -1$ with $\phi = 0$ or $T_1 = -T_2 = \pm 1$. Here, we develop predictions for $\{P(I), P(U), P(Q), P(V)\}$ in terms of waves in n pairs of orthonormal modes. The ith wave population is described by axial ratio T_i, polarization angle ϕ_i, field strength PDF $P(E_i)$, and phase PDF $P(\Phi_i)$.

B. Earlier models of polarization statistics

It is almost 60 years since Hurwitz [7] first described the statistics of unpolarized light: showing that the combination of E_x and E_y component wave populations with identical zero-mean Gaussian distributions for the fields yields a Gamma distribution for the total intensity, and a uniform distribution for the total degree of circular polarization. Since that time research into the statistical properties of polarized light and the Stokes parameters has steadily advanced (e.g., see [25] and references therein). Salient research includes that of Barakat [8,9], who extended the analysis of Hurwitz to study the statistics of partially polarized light, and more recently that of Eliyahu [10], who showed that the analytic expressions could be written more compactly by normalizing to the intensity.

Eliyahu represented the electric field in terms of E_x and E_y component wave populations, with a joint PDF $P(|E_x|, |E_y|, \Phi_x, \Phi_y)$ which is nonseparable in the field strengths $|E_x|$ and $|E_y|$. Using a change of variables, integration over the real part of E_y, and the conditional probability $P(I | U, Q, V) = \delta(I - \sqrt{U^2 + Q^2 + V^2})$, an expression for the joint PDF $P(I, U, Q, V)$ of the Stokes parameters was obtained. Finally, integration over the Stokes parameters yields expressions for $P(S)$ in terms of S and its first-order moments. This approach can sometimes yield simpler boundaries of integration as compared to the integration over the electric fields and phase differences performed here, but with the disadvantage that the properties of the predicted distribution function cannot be simply related to those of the components. A comparison between approaches is outside the scope of this work. Importantly, however, if the plasma modes are linearly polarized then the E_x and E_y components in Eliyahu are simply related to those of the plasma. In this case, and providing the average value of V is zero, the joint PDF is separable in the field strengths, and the analyses match.

In summary, the analyses of Hurwitz [7], Barakat [8,9], and Eliyahu [10] differ from this work in two fundamental respects. First, the representation of the electric field by superposing E_x and E_y fields with different field strength distributions has, in general, no simple interpretation in terms of the component modes of the plasma. The exception is for the superposition of linearly polarized modes in which the average value of V is zero. In this instance, Eliyahu's analysis is a special case of our more general treatment. Second, Hur-

witz, Barakat, and Eliyahu used a Gaussian PDF with zero mean for each field strength. While only examples of the combination of lognormal field distributions are presented later, in the present work our method is not restricted to a particular field strength distribution.

III. STOKES PARAMETERS FOR THE SUPERPOSITION OF TWO STOCHASTIC WAVE POPULATIONS

A. Integral expressions for the PDFs of the polarization parameters

While in this work we compute predictions only for the Stokes parameters resulting from the vector superposition of orthonormal mode pairs, it is nonetheless useful to retain the formalism for the superposition of arbitrarily polarized pairs. The advantage is that this generalization provides an analytic description of the superposition of two pairs of orthonormal modes in which each mode pair has a dominant component. Without loss of generality, the $(\mathbf{e}_x, \mathbf{e}_y)$ coordinate axis can be rotated such that the electric field of one wave may be written in the axial-ratio formulation [Eq. (3)]. The second wave vector can then be written in the frame of the first. In matrix notation,

$$\mathbf{E}_1 = \frac{E_1 e^{i(\Phi_1 - \omega t)}}{\sqrt{1+T_1^2}} \begin{pmatrix} T_1 & i \end{pmatrix} \begin{pmatrix} \mathbf{e}_x \\ \mathbf{e}_y \end{pmatrix}, \tag{23}$$

$$\mathbf{E}_2 = \frac{E_2 e^{i(\Phi_2 - \omega t)}}{\sqrt{1+T_2^2}} \begin{pmatrix} T_2 & i \end{pmatrix} \begin{pmatrix} \cos\phi & \sin\phi \\ -\sin\phi & \cos\phi \end{pmatrix} \begin{pmatrix} \mathbf{e}_x \\ \mathbf{e}_y \end{pmatrix}. \tag{24}$$

The Stokes parameters for the superposition of the two modes can then be computed, yielding

$$I = E_1^2 + E_2^2 + E_1 E_2 \left[\frac{(T_1+1)(T_2+1)}{\sqrt{(T_1^2+1)(T_2^2+1)}} \cos(\phi + \Phi_1 - \Phi_2) + \frac{(T_1-1)(T_2-1)}{\sqrt{(T_1^2+1)(T_2^2+1)}} \cos(\phi - \Phi_1 + \Phi_2) \right], \tag{25}$$

$$Q = E_1^2 \left(\frac{T_1^2-1}{T_1^2+1} \right) + E_2^2 \left(\frac{T_2^2-1}{T_2^2+1} \right) \cos 2\phi + E_1 E_2 \left[\frac{(T_1-1)(T_2+1)}{\sqrt{(1+T_1^2)(1+T_2^2)}} \cos(\phi + \Phi_1 - \Phi_2) + \frac{(T_1+1)(T_2-1)}{\sqrt{(1+T_1^2)(1+T_2^2)}} \cos(\phi - \Phi_1 + \Phi_2) \right], \tag{26}$$

$$U = E_2^2 \left(\frac{T_2^2-1}{T_2^2+1} \right) \sin 2\phi + E_1 E_2 \left[\frac{(T_1-1)(T_2+1)}{\sqrt{(1+T_1^2)(1+T_2^2)}} \times \sin(\phi + \Phi_1 - \Phi_2) + \frac{(T_1+1)(T_2-1)}{\sqrt{(T_1^2+1)(T_2^2+1)}} \times \sin(\phi - \Phi_1 + \Phi_2) \right], \tag{27}$$

$$V = \frac{2E_1^2 T_1}{1+T_1^2} + \frac{2E_2^2 T_2}{1+T_2^2} + E_1 E_2 \left[\frac{(T_1+1)(T_2+1)}{\sqrt{(T_1^2+1)(T_2^2+1)}} \times \cos(\phi + \Phi_1 - \Phi_2) - \frac{(T_1-1)(T_2-1)}{\sqrt{(T_1^2+1)(T_2^2+1)}} \times \cos(\phi - \Phi_1 + \Phi_2) \right]. \tag{28}$$

Thus, each Stokes parameter S can be written

$$S = \alpha_S(T_1, \phi) E_1^2 + \beta_S(T_2, \phi) E_2^2 + \gamma_S(T_1, T_2, \phi, \psi) E_1 E_2 \tag{29}$$

with $\alpha_S(T_1)$, $\beta_S(T_1)$, and $\gamma_S(T_1, T_2, \phi, \psi)$ representing the coefficients of E_1^2, E_2^2, and $E_1 E_2$ in Eqs. (25)–(28), and where $\psi \equiv \Phi_1 - \Phi_2$ is the difference in phases. For simplicity, the S subscript is omitted where not needed below. Using the method described in Sec. II, integral forms for the Stokes PDFs for two sources can be written

$$P(S) = \int \frac{P(\psi) P(E_1^2) P(E_2^2) dE_1^2 dE_2^2}{\left| \frac{\partial(S, E_1^2, E_2^2)}{\partial(\psi, E_1^2, E_2^2)} \right|} \tag{30}$$

$$= \int \frac{P(\psi) P(E_1^2) P(E_2^2) dE_1^2 dE_2^2}{\left| E_1 E_2 \frac{\partial \gamma}{\partial \psi} \right|}, \tag{31}$$

where

$$\left| \frac{\partial(S, E_1^2, E_2^2)}{\partial(\psi, E_1^2, E_2^2)} \right| = \begin{vmatrix} \partial S/\partial\psi & \partial S/\partial E_1^2 & \partial S/\partial E_2^2 \\ \partial E_1^2/\partial\psi & \partial E_1^2/\partial E_1^2 & \partial E_1^2/\partial E_2^2 \\ \partial E_2^2/\partial\psi & \partial E_2^2/\partial E_1^2 & \partial E_2^2/\partial E_2^2 \end{vmatrix} = \left| E_1 E_2 \frac{\partial \gamma}{\partial \psi} \right| \tag{32}$$

has been used. For given S, E_1, and E_2 there are two solutions for ψ: hence $\partial\gamma/\partial\psi$ takes both positive and negative values. When integrating over the field strengths, care must be taken to include both solutions. For the degree of circular polarization,

$$P(v) = \int \frac{P(\psi) P(E_1^2) P(E_2^2) dE_1^2 dE_2^2}{|(E_1 E_2 / I)(\partial \gamma_V / \partial \psi - v \partial \gamma_I / \partial \psi)|}. \tag{33}$$

Finally, as the component wave populations are fully polarized, it follows that the superposed wave population will also be fully polarized (i.e., have an interpretation in terms of the Poincaré sphere). That is, the degree of linear polarization is related to the degree of circular polarization through Eq. (8), recast as

$$r_l^2 + v^2 = 1. \tag{34}$$

The PDF of the degree of linear polarization $r_l = \sqrt{U^2+Q^2}/I$ can thus be computed directly from the PDF of the degree of circular polarization $P(v)$ through a change of variable

$$P(r_l) = P(v) \Big/ \left| \frac{\partial r_l}{\partial v} \right| \tag{35}$$

$$=[P(v)+P(-v)]\left|\frac{\sqrt{1-v^2}}{v}\right|. \tag{36}$$

B. Properties of the distribution functions

With expressions for $P(S)$ and $P(v)$ determined, it is convenient to introduce a new subscript notation for the PDF [e.g., P_S for $P(S)$], used hereafter to distinguish the PDF from its argument. Prior to computation of P_S, it is worth noting that certain properties of the distribution function do not require quantitative calculation of the PDF. The qualitative behavior of P_S at very small and very large $|S|$ values can be probed by studying the ranges of $\alpha(T_1)$, $\beta(T_2)$, and $\gamma(T_1,T_2,\phi,\psi)$ in Eq. (29). These terms satisfy the inequalities $|\alpha|\leqslant 1$, $|\beta|\leqslant 1$, and $|\gamma|\leqslant 2$. Hence, for given E_1 and E_2, S lies in the interval

$$(\alpha-1)E_1^2+(\beta-1)E_2^2+(E_1-E_2)^2\leqslant S\leqslant(E_1+E_2)^2. \tag{37}$$

For I, $\alpha=\beta=1$, and so inequality (37) reduces to $(E_1-E_2)^2 \leqslant I\leqslant(E_1+E_2)^2$. This reveals a possible difference in behavior of P_I between low and large I values. For I values approaching $(E_1-E_2)^2$, P_I samples P_{E_1} and P_{E_2} across a wide range of field strengths. In contrast, for I values approaching $(E_1+E_2)^2$, P_I samples P_{E_1} and P_{E_2} chiefly at high field strengths. Similar behavior is expected for P_U, P_Q, and P_V at small and large $|S|$ values. For small $|S|$ there exist T_1, T_2, ϕ, and ψ values such that P_S samples P_{E_1} and P_{E_2} over a wide range of field strengths. In contrast, at high $|S|$, P_S samples P_{E_1} and P_{E_2} chiefly at high field strengths.

If the phases are random with a uniform distribution $P_{S\psi}(\psi)=1/2\pi$, the mean of the Stokes parameters for two wave populations can be computed as follows:

$$\langle S\rangle=\int\int\int S(E_1,E_2,\psi)P_S(E_1,E_2,\psi)dE_1dE_2d\psi \tag{38}$$

$$=\int\int\int[\alpha E_1^2+\beta E_2^2+\gamma(\psi)E_1E_2] \times P_{SE_1}(E_1)P_{SE_2}(E_2)P_{S\psi}(\psi)dE_1dE_2d\psi \tag{39}$$

$$=\langle S_1\rangle+\langle S_2\rangle, \tag{40}$$

where the integral $\int\gamma(\psi)P_{S\psi}(\psi)d\psi=0$ because $\gamma(\psi)$ is trigonometric. Here, the PDF $P_S(E_1,E_2,\psi)$ is the joint probability of E_1, E_2, and ψ.

Generalization of Eq. (40) to the result

$$\langle S\rangle=\sum_i^n\langle S_i\rangle \tag{41}$$

for multiple random phase sources is straightforward. The result does *not* extend to expectation values for the degrees of circular and linear polarization, because the integrals of the cross field terms (e.g., E_1E_2) in Eq. (38) are not zero.

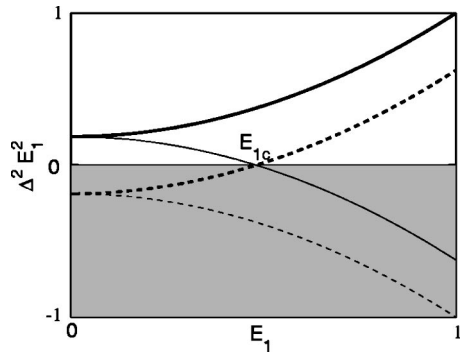

FIG. 2. Schematic plot of $\Delta^2E_1^2$, with Δ given by Eq. (43). The solid curves show $\gamma^2-4\alpha\beta>0$ (thick) and $\gamma^2-4\alpha\beta<0$ (thin) for $4\beta S>0$, the dashed curves show $\gamma^2-4\alpha\beta>0$ (thick) and $\gamma^2-4\alpha\beta<0$ (thin) for $4\beta S<0$. Unphysical solutions lie in the shaded region.

C. Boundaries of integration

Calculation of the PDFs through integration over E_1^2 and E_2^2 first requires the boundaries of integration in Eqs. (31) and (33) to be established. For simplicity, we hereafter refer to the parameter space defined by E_1 and E_2 as E space. For a given E_1, we note that each Stokes equation [Eqs. (25)–(28)] is a quadratic in E_2 with only one unknown, $\psi\equiv\Phi_1-\Phi_2$. In general, each Stokes equation of form given by Eq. (29) can thus be solved for E_2, giving

$$E_2=E_1\left(\frac{-\gamma(T_1,T_2,\psi)\pm\Delta(E_1,S)}{2\beta(T_2)}\right). \tag{42}$$

Physical solutions for E_2 require the discriminant

$$\Delta(E_1,S)=\sqrt{\gamma(T_1,T_2,\psi)^2-4\beta(T_2)[\alpha(T_1)E_1^2-S]/E_1^2} \tag{43}$$

to be real and positive, which yields constraints on E_1. That is, $\Delta(E_1,S)^2E_1^2$ is a quadratic in E_1, with possible loci shown in Fig. 2. Unphysical solutions lie in the shaded region. The solid curves correspond to $\gamma^2-4\alpha\beta>0$ (thick curve) and $\gamma^2-4\alpha\beta<0$ (thin curve) for $4\beta S>0$, in which case either E_1 is unbounded or $E_1<E_{1c}$. The dashed curves correspond to $\gamma^2-4\alpha\beta>0$ (thick) and $\gamma^2-4\alpha\beta<0$ (thin) for $4\beta S<0$, in which case either $E_1>E_{1c}$ or the boundary vanishes (i.e., E_1 cannot take any value). The corresponding cutoff is

$$E_{1c}(\psi)=\sqrt{\left|\frac{4\beta(T_2)S}{4\alpha(T_1)\beta(T_2)-\gamma(T_1,T_2,\psi_c)^2}\right|}. \tag{44}$$

Extrema in $E_{1c}(\psi)$ lie at ψ solutions of $\partial\gamma/\partial\psi=0$. The solution $\gamma=0$ does not correspond to a maximum in E_{1c}.

For fixed E_1, S, T_1, T_2, and ϕ upper and lower bounds of E_2 can be found by locating solutions of $dE_2/d\psi=0$; these occur at

$$\frac{dE_2}{d\psi}=-E_1E_2\frac{\partial\gamma}{\partial\psi}\Big/(2\beta E_2+E_1\gamma)=0. \tag{45}$$

Neglecting the special cases $E_1=0$, $E_2=0$, or $2\beta E_2+E_1\gamma=\infty$, solutions for Eq. (45) lie at

$$\tan\psi_I = -\left(\frac{T_1+T_2}{1+T_1T_2}\right)\tan\phi, \tag{46}$$

$$\tan\psi_U = \left(\frac{T_1-T_2}{T_1T_2-1}\right)\cot\phi, \tag{47}$$

$$\tan\psi_Q = \left(\frac{T_2-T_1}{T_1T_2-1}\right)\tan\phi, \tag{48}$$

$$\tan\psi_V = -\left(\frac{1+T_1T_2}{T_1+T_2}\right)\tan\phi. \tag{49}$$

Finally, we note that the functions $\tan\psi$ and $\tan\gamma$ are π periodic, so there are two solutions with $-\pi<\psi\leqslant\pi$ for which $\partial\gamma/\partial\psi=0$, corresponding to four solutions for E_2. Two of these solutions are negative, and can therefore be discarded. To remove the degeneracy of ψ_S over a 2π interval, we arbitrarily label the solution lying at $\gamma<0$ as $\psi=\psi_S$ with $\gamma^-=\gamma(\psi_S)$, and label the solution lying at $\gamma>0$ as $\psi=\psi_S\pm\pi$ with $\gamma^+=\gamma(\psi_S\pm\pi)$. The remaining physical solutions for E_2 yield the constraints

$$\frac{|\gamma^-|-\Delta}{2|\beta|} \leqslant \frac{E_2(\beta>0,\Delta^2<\gamma^2)}{E_1} \leqslant \frac{|\gamma^-|+\Delta}{2|\beta|}, \tag{50}$$

$$\frac{-|\gamma^+|+\Delta}{2|\beta|} \leqslant \frac{E_2(\beta>0,\Delta^2>\gamma^2)}{E_1} \leqslant \frac{|\gamma^-|+\Delta}{2|\beta|}, \tag{51}$$

$$\frac{-|\gamma^-|+\Delta}{2|\beta|} \leqslant \frac{E_2(\beta<0,\Delta^2>\gamma^2)}{E_1} \leqslant \frac{|\gamma^+|+\Delta}{2|\beta|}, \tag{52}$$

$$\frac{|\gamma^+|-\Delta}{2|\beta|} \leqslant \frac{E_2(\beta<0,\Delta^2<\gamma^2)}{E_1} \leqslant \frac{|\gamma^+|+\Delta}{2|\beta|}. \tag{53}$$

For a given E_1, α, β, and S the upper and lower solutions to E_2 therefore satisfy $\psi=\psi_c$ and $\psi=\psi_c\pm\pi$, respectively.

In summary, both E_1 and E_2 integration boundaries can hence be parametrized by solutions of $\partial\gamma/\partial\psi=0$; i.e., $E_1\geqslant E_{1c}(\psi_c)$ or $E_1\leqslant E_{1c}(\psi_c)$, and

$$f_l(E_1,\psi_c) \leqslant E_2 \leqslant f_u(E_1,\psi_c), \tag{54}$$

where $f_l(E_1,\psi_c)$, $f_u(E_1,\psi_c)$ are the upper (+) and lower (−) physical solutions to Eq. (42). The angle ψ_c is that which maximizes the domain of integration in both E_1 and E_2. For instance, if $\phi=0$, then $\psi_I=0,\pi$ for I, corresponding to vector parallel and antiparallel addition. If $T_1=T_2$, then $E_{1c}(\psi_c)=\infty$, and

$$\{E_1^2>I\},\ \ E_1-\sqrt{I}\leqslant E_2\leqslant E_1+\sqrt{I}, \tag{55}$$

$$\{E_1^2<I\},\ \ -E_1+\sqrt{I}\leqslant E_2\leqslant E_1+\sqrt{I}. \tag{56}$$

These were the boundary conditions used by Cairns *et al.* [23] in their investigation of the intensity statistics of two vectorially superposed wave populations where the boundaries $E_2=E_1\pm\sqrt{I}$ correspond to antiparallel vector addition, and $E_2=\sqrt{I}-E_1$ to parallel vector addition. Indeed, provided that the polarization angle and axial ratio of the two modes are identical ($\phi=0$ and $T_1=T_2$, respectively), our analysis for P_I reduces to that of Cairns *et al.* [23].

By locating zeros of $\partial\psi/\partial E_2$, the boundaries in ψ can be similarly studied. For constant E_1, ϕ, T_1, T_2, and S, $\partial\psi/\partial E_2=1/\partial E_2/\partial\psi$, and so from Eq. (45) zeros of $\partial\psi/\partial E_2$ lie at $\gamma=-2\beta E_2/E_1$. Using Eq. (42) for E_2 we find that the zeros of $d\psi/dE_2$ correspond to real solutions of

$$\gamma = -2\frac{\beta}{|\beta|}\sqrt{\alpha\beta-\beta S/E_1^2}. \tag{57}$$

Immediately, we note that either $E_1^2\geqslant S/\alpha$ for $\beta>0$ for $E_1^2\leqslant S/\alpha$ for $\beta<0$ must also be satisfied for a zero in $d\psi/dE_2$ to exist. As the function $\gamma(\psi)$ represents a superposition of sine and/or cosine functions of the same periodicity, it can always be represented as a single sine or cosine function of an appropriately shifted ψ. Given that $\gamma(\psi)$ is a local minimum at $\psi=\psi_S$, we conclude $\gamma(\psi'=\psi-\psi_S)$ will be an even function of ψ'. Finally, using Eqs. (25)–(28) to substitute for γ, Eq. (57) can be solved for ψ and hence ψ'.

Boundaries in (E_1,E_2) and ψ can similarly be established for the degree of circular polarization $v=V/I$. For brevity, we list only salient differences to the S boundaries. For a given E_1, T_1, T_1, and ϕ, the equation $v=V/I$ can be rearranged as a quadratic in E_2 with only one unknown: ψ'. That is,

$$E_2^2\overline{\beta}(\psi')+E_2E_1\overline{\gamma}(\psi')+E_1^2\overline{\alpha}(\psi')=0, \tag{58}$$

where $\overline{\alpha}(\psi')=\alpha_V-v(\psi')\alpha_I$, $\overline{\beta}(\psi')=B_V-v(\psi')\beta_I$, and $\overline{\gamma}(\psi')=\gamma_V(\psi')-v(\psi')\gamma_I(\psi')$. Equation (58) is homogeneous in the field strengths, and so two conclusions follow: E_2 boundaries are straight lines through the origin, and zeros of $d\psi/dE_2$ lie at $\overline{\gamma}=-2(\overline{\beta}/|\overline{\beta}|)\sqrt{\overline{\alpha}\overline{\beta}}$, similar to Eq. (57) with $\alpha\leftrightarrow\overline{\alpha}$, $\beta\leftrightarrow\overline{\beta}$, and $S\leftrightarrow 0$.

D. Limiting properties of the integrand

The PDFs $P(\psi)$, $P(E_1^2)$, and $P(E_2^2)$ are all finite, whereas the Jacobian $|E_1E_2\partial\gamma/\partial_\psi|$ for $P(S)$ has zeros at $\psi=\psi_c$, $E_1=0$, and $E_2=0$. In this work, the behavior of the Jacobian is examined by an expansion of E_2^2 and $\partial\gamma/\partial\psi$ about the boundary $\psi=\psi_c$. This yields a limiting form for the Jacobian along an E_2 interval of fixed E_1 local to the $\psi=\psi_c$ boundary. The limiting behavior along an E_1 interval with fixed E_2 is then obtained by interchanging the E_1 and E_2 labels. We also note that the values $E_1=0$ and $E_2=0$ correspond to points along the boundary $\psi=\psi_c$, and are hence implicitly included in a $\psi=\psi_c$ expansion.

Noting that the boundary $\psi=\psi_c$ is defined by solutions to $\partial\gamma/\partial\psi=0$, expansions of E_2^2 and $\partial\gamma/\partial\psi$ about $\psi=\psi_c$ (where $\partial E_2/\partial\psi=0$) to second order in $\psi-\psi_c$ can be written

$$E_2^2 = E_{2c}^2+\left\{\frac{\partial^2E_2^2}{\partial\psi^2}\right\}_{\psi_c}(\psi-\psi_c)^2 \tag{59}$$

$$=E_{2c}^2+\left\{2E_2\frac{\partial}{\partial\psi}\left(\frac{\partial E_2}{\partial\gamma}\frac{\partial\gamma}{\partial\psi}\right)\right\}_{\psi_c}(\psi-\psi_c)^2 \tag{60}$$

$$= E_{2c}^2 + \left\{ \frac{2}{E_2}\frac{\partial E_2}{\partial \gamma}\frac{\partial^2 \gamma}{\partial \psi^2} \right\}_{\psi_c} E_2^2 (\psi - \psi_c)^2 \tag{61}$$

and

$$\frac{\partial \gamma}{\partial \psi} = \left\{ \frac{\partial^2 \gamma}{\partial \psi^2} \right\}_{\psi_c} (\psi - \psi_c). \tag{62}$$

Rearranging Eq. (61) we find,

$$\left\{ \frac{\partial^2 \gamma}{\partial \psi^2} \right\}_{\psi_c} (\psi - \psi_c)^2 = \left(\frac{\partial \gamma}{\partial \psi} \right)^2 \Bigg/ \left\{ \frac{\partial^2 \gamma}{\partial \psi^2} \right\}_{\psi_c}, \tag{63}$$

to $O(\psi - \psi_c)^2$, since $\partial\gamma/\partial\psi$ is itself of $O(\psi - \psi_c)$. Consequently, Eq. (61) can be rewritten as

$$E_2^2 = E_{2c}^2 + \left\{ \frac{2}{E_2}\frac{\partial E_2}{\partial \gamma} \Bigg/ \frac{\partial^2 \gamma}{\partial \psi^2} \right\}_{\psi_c} E_2^2 \left(\frac{\partial \gamma}{\partial \psi} \right)^2. \tag{64}$$

Near the boundaries of integration, we find that the integrand of Eq. (31) thus obeys

$$\lim_{\psi \to \psi_c} \frac{P(\psi) P(E_1^2) P(E_2^2)}{|E_1 E_2 \partial\gamma/\partial\psi|} \propto \lim_{\psi \to \psi_c} \frac{P(\psi) P(E_1^2) P(E_2^2)}{|E_1 \sqrt{|E_2^2 - E_{2c}^2|}|}. \tag{65}$$

Therefore, we conclude that for fixed E_1 the integrand contains a square-root singularity at the boundary $E_2^2 = E_{2c}^2$. Interchanging the labels in the above analysis, we find that for fixed E_2, the integrand also contains a square-root singularity at $E_1^2 = E_{1c}^2$. Limiting properties of the Jacobian for $P(v)$ can be similarly studied, also yielding a square-root singularity as $\psi \to \psi_v$ at the E_1 and E_2 boundaries.

E. Numerical integration

Equations (31) and (33) contain integrals with square-root singularities at the boundaries, E_{1c} and E_{2c}. To compute the integrals, a Romberg [23,26] integration procedure was used together with a change of variables at the singularities. To ensure convergence, each E_1 and E_2 interval was subdivided into $\log_n E_{\max}/E_{\min}$ intervals, and a change of variable used at the overall lower and upper boundaries. For the results presented in this work, $n = 10$ was used.

To compute P_S for each value of S, the integrand of Eq. (31) must be evaluated for every E_1 and E_2: this requires solutions for ψ to Eq. (29) to be found. Solutions for ψ were determined by calculating γ from

$$\gamma = \frac{S - \alpha E_1^2 - \beta E_2^2}{E_1 E_2}, \tag{66}$$

equating to the $E_1 E_2$ coefficient for γ in Eqs. (25)–(28), rearranging as a quadratic in $\cos\psi$, and solving for $\cos\psi$ and ψ. Two solutions to $\cos\psi$ are obtained, and thus four solutions to ψ over a 2π interval. Finally, when computing the contribution to $P(S)$ in Eq. (31), the two physical solutions to S are selected and the integrand summed over both solutions.

For P_v the procedure involves rearranging the equation

$$\overline{\gamma} = \frac{-\alpha E_1^2 - \beta E_2^2}{E_1 E_2} = \frac{(T_1 + 1)(T_3 + 1)}{\sqrt{(T_1^2 + 1)(T_3^2 + 1)}}(1 - v)\cos(\phi + \psi) - \frac{(T_1 - 1)(T_3 - 1)}{\sqrt{(T_1^2 + 1)(T_3^2 + 1)}}(1 + v)\cos(\phi - \psi) \tag{67}$$

as a quadratic in $\cos\psi$, solving for ψ, and summing the integrand of Eq. (33) over the two ψ solutions.

IV. ILLUSTRATIONS FOR THE VECTOR SUPERPOSITION OF ORTHONORMAL MODES

In this section we compute PDFs for the polarization properties of the superposition of two orthonormal modes. For $\phi = 0$ and $T_1 T_2 = -1$ the Stokes parameters [Eqs. (25)–(28)] reduce to

$$I = E_1^2 + E_2^2, \tag{68}$$

$$Q = (E_1^2 - E_2^2)\left(\frac{T_1^2 - 1}{T_1^2 + 1} \right) - 2E_1 E_2 \frac{T_1}{|T_1|}\left(\frac{2T_1}{T_1^2 + 1} \right)\cos\psi, \tag{69}$$

$$U = 2E_1 E_2 \frac{T_1}{|T_1|}\sin\psi, \tag{70}$$

$$V = (E_1^2 - E_2^2)\left(\frac{2T_1}{1 + T_1^2} \right) + 2E_1 E_2 \frac{T_1}{|T_1|}\left(\frac{T_1^2 - 1}{T_1^2 + 1} \right)\cos\psi. \tag{71}$$

Immediately, we note that the PDF for the intensity I is reduced to a simple convolution of field strengths:

$$P_I = \int P_{E1}(I - E_2^2) P_{E2}(E_2^2) dE_2^2. \tag{72}$$

When the modes are have identical axial ratios and the same polarization angle (not orthonormal), P_I is not given by the convolution in Eq. (72). Instead, the detailed analysis of Cairns *et al.* [23] follows.

For orthonormal modes ($T_1 T_2 = -1$) the expressions for V and Q are related by the field interchange mapping

$$\overline{E_1} \leftrightarrow E_2, \tag{73}$$

$$\overline{E_2} \leftrightarrow E_1, \tag{74}$$

$$\frac{\overline{T_1^2} - 1}{2\overline{T_1}} \leftrightarrow \frac{2T_1}{T_1^2 - 1}, \tag{75}$$

$$\frac{\overline{T_1}}{|\overline{T_1}|} \leftrightarrow \frac{T_1}{|T_1|}, \tag{76}$$

under which $\overline{Q} \leftrightarrow V$ and so $P_{\overline{Q}} \leftrightarrow P_V$.

In this work, various combinations of the orthonormal wave populations in Table I are superposed for illustrative

TABLE I. Illustrative lognormal wave population field characteristics, and polarizations. The two components in cases (i), (iii), and (v) have equal field strength distributions, with mean and standard deviation $\mu_A = 1.2 \ln 10$, $\sigma_A^2 = 0.2 \ln 10$, while the two components in cases (ii), (iv), and (vi) have unequal field strengths, where the second component is dominant with $\mu_B = 2.1 \ln 10$, $\sigma_B^2 = 0.1 \ln 10$.

	Elliptic		Circular		Linear	
	(i)	(ii)	(iii)	(iv)	(v)	(vi)
T_1	0.5	0.5	1	1	∞	∞
T_2	−2	−2	−1	−1	0	0

purposes. While the theory is developed for an arbitrary choice of distribution function, for illustrative purposes, we have chosen lognormal field strength distributions function, for E_1 and E_2. The six cases correspond to calculations for the different polarization states (elliptical, circular, and linear) performed for two pairs of wave populations. One wave pair has a dominant (more intense) population and a weaker population, whereas the other case has two identical wave populations. The field strength distributions have been chosen to allow direct comparison with earlier vector convolution calculations [23]. The case of circular mode polarization is particularly relevant for the propagation of electromagnetic modes in free space, which propagate as oppositely circularly polarized waves with the same refractive index [5].

A. Boundaries of integration

Prior to calculation of P_I, P_U, P_Q, P_V, and P_v the boundaries of integration in E space must be computed using the analytic procedures described in Sec. III. For orthonormal modes, P_I reduces to a line integral in (E_1, E_2) space, with $E_1 = \sqrt{I - E_2^2}$. For P_V, P_Q, P_U, and P_v we illustrate the boundaries for a few selected values from the orthonormal modes of Table I. Importantly, the boundaries in E space are independent of the choice of field strength and phase difference distributions. Some properties of the boundaries are also further described in Sec. IV B when describing features of the distribution functions.

1. Elliptically polarized modes

For cases (i) and (ii) $\alpha_V > 0$, $\beta_V < 0$, so the boundaries for P_V are described analytically by the intervals (52) and (53). Figure 3(a) plots the boundaries of integration in (E_1, E_2) space for $P_V(V=5)$ in cases (i) and (ii). For convenience, we hereafter drop the value assignment within the brackets, so that $P_S(5)$ is shorthand for $P_S(S=5)$. In Fig. 3(a) contours of equal $|\psi'| = |\psi - \psi_V|$ are drawn. The gray scale at the top of Fig. 3(a) identifies the value of $|\psi - \psi_V'|$ in (a), and the solid lines define the analytic boundary. In Figs. 3(b) and 3(c) the corresponding $|\psi'|$ domain is plotted against E_1 and E_2, respectively. In Fig. 3(b) with $E_1 = 2.4$, for instance, solutions for E_2 of Eq. (71) can only be found providing $|\psi - \psi_V'|$ lies in the range $1.97 < |\psi - \psi_V'| \leq \pi$. In Fig. 3(c) with $E_2 = 2.4$, however, solutions for E_1 of Eq. (71) can be found for any $|\psi - \psi_V'| < \pi$.

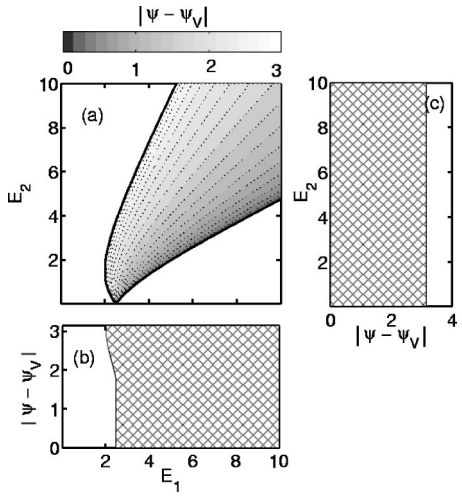

FIG. 3. (a) Contour plot of the integration boundaries in E space for $V=5$ for the elliptically polarized modes of cases (i) and (ii). The horizontal gray scale denotes the value of $|\psi'| = |\psi - \psi_V|$, and the solid thick line shows the analytic boundaries of integration. The hatched regions in (b) and (c) describe the integrable range of $|\psi'|$ as functions of E_1 and E_2, respectively.

Inspection of inequality (50) shows that the stationary points of γ_V are located at $\psi = 0, \pi$ with $\psi_V = 0$ the solution that minimizes γ_V. For $E_1 \leqslant \sqrt{V/\alpha}$, the lower and upper E_2 boundaries lie on the $|\psi'| = \pi$ contour [see Eq. (53)]. For $E_1 \geqslant \sqrt{V/\alpha}$ the lower and upper E_2 boundaries lie on the $|\psi'| = 0$ and $|\psi'| = \pi$ contours [see Eq. (52)]. This explains why the $|\psi|$ domain in Fig. 3(b) for $E_1 \leqslant \sqrt{(V/\alpha)}$ is local to $|\psi| = \pi$. Finally, under the field interchange mapping $\overline{E_1} \leftrightarrow E_2$, $\overline{E_2} \leftrightarrow E_1$, $\overline{T_1} \leftrightarrow T_2$, $\overline{T_2} \leftrightarrow T_1$, with $\overline{\psi'} \leftrightarrow \psi' + \pi$, we obtain $\overline{V} = -V$, so the boundary for $V=-5$ is a reflection of the $V=5$ boundary through $E_1 = E_2$. The domain for $\overline{\psi'}$ as a function of E_2 is identical to that in Fig. 3(b), with $\psi_V = \pi$. Similarly, the domain for $\overline{\psi'}$ as a function of E_1 is identical to that in Fig. 3(c).

Due to the field interchange mapping of Eqs. (73)–(76), under which $\overline{Q} = V$, the boundaries for Q are related to those of V: the boundary for $Q=-5$ is similar to that of $V=+5$, and the boundary for $Q=5$ a reflection of $Q=-5$. Finally, for U, the coefficients $\alpha_U = \beta_U = 0$, and so the boundary of integration is described by the hyperbola $|U| = 2E_1E_2$.

For the degree of circular polarization, Eq. (67) simplifies to

$$\overline{\gamma} = 2\frac{T_1}{|T_1|}\left(\frac{T_1^2 - 1}{T_1^2 + 1}\right)\cos\psi. \tag{77}$$

Stationary points of $\overline{\gamma}$ lie at $\psi = 0, \pi$, with $\psi_v = \pi$ the solution that minimizes Eq. (77). For cases (i) and (ii) with $v = 0.85$, $\overline{\alpha} < 0$ and $\overline{\beta} < 0$, so the boundaries for E_2 are described analytically by the interval (53), with $\beta \leftrightarrow \overline{\beta}$, $\gamma \leftrightarrow \overline{\gamma}$, and $\overline{\Delta} = \overline{\gamma}^2 - 4\overline{\alpha}\overline{\beta}$. Figure 4(a) plots the boundaries of integration for $P_v(0.85)$ for cases (i) and (ii). In these instances the lower

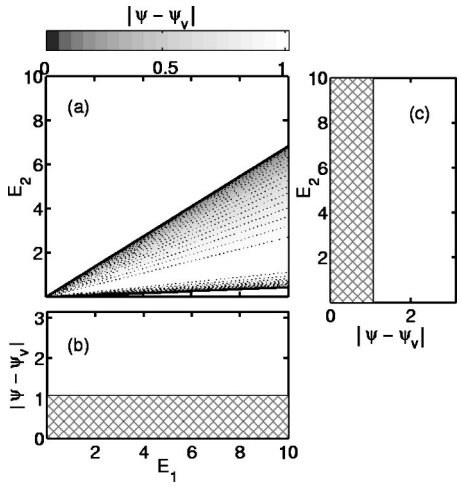

FIG. 4. Similar to Fig. 3 but showing the integration boundaries in E space for $v=0.85$, together with the ranges of $|\psi'|$ as functions of E_1 and E_2.

and upper boundaries are both described by the $\psi'=0$ contour, and so ψ' solutions are degenerate over a π interval. Physically, the two different solutions at common ψ' and E_1 values in Fig. 4(a) trace polarization ellipses with the same T, but different intensity and polarization angle. Analytically, this degeneracy will occur whenever $\Delta^2<\overline{\gamma}^2$, given by the upper and lower boundary intervals of (50) and (53), with $\beta\leftrightarrow\overline{\beta}$, $\gamma\leftrightarrow\overline{\gamma}$, and $\overline{\Delta}\leftrightarrow\Delta$. For orthonormal modes, the use of $\overline{\Delta}^2<\overline{\gamma}^2$ yields $v^2>v(v_1+v_2)-v_1v_2=v_1^2$, where v_1 and $v_2=-v_1$ are the degrees of circular polarization of the two component waves. That is, ψ' solutions will be degenerate over a π interval whenever the magnitude of the total degree of polarization is larger than the magnitude of the degree of circular polarization of either mode. A similar fourfold ψ degeneracy can occur for local regions in E space for V and Q, where $\Delta(E_1)^2<\gamma^2$ [e.g., the $E_1\leqslant\sqrt{V/\alpha}$ region in Fig. 3(a)]. Excepting $S=0$, however, it is only for v that the degeneracy extends over all E space, where the E_1 dependence of $\overline{\Delta}$ vanishes.

The $|\psi'|$ domain, shown versus E_1 and E_2 in Figs. 4(b) and 4(c), respectively, can be quantitatively determined by equating the solutions of $d\psi/dE_2=0$ [given by $\overline{\gamma}=-2\overline{\beta}/\overline{\beta}\sqrt{\overline{\alpha}\overline{\beta}}$], to Eq. (77), and solving for ψ'. For cases (i) and (ii) this yields $\psi'<\arccos[\sqrt{\overline{\alpha}\overline{\beta}}(T_1^2+1)/(T_1^2-1)]\simeq\pi/3$. More generally, for the degree of circular polarization of arbitrary orthonormal modes, the discriminant $\overline{\Delta}^2$ reduces to $\overline{\Delta}^2=4(v^2-1)$ at the boundaries ($\psi'=0,\pi$). At these locations, $|v|=1$, and so the expression for P_v reduces to a line integral over $E_2=E_1\overline{\gamma}/(2\overline{\beta})$.

2. Circularly and linearly polarized modes

Expressions for the Stokes parameters I and U arising from the superposition of circular and linear polarization waves [cases (iii)–(vi) in Table I] are identical to the preceding results for elliptical polarization. For circularly and linearly polarized waves, expressions for Q and V are simply related: $Q(T_1=1)=-V(T_1=\infty)=-2E_1E_2\cos\psi$, and $Q(T_1=\infty)=V(T_1=1)=E_1^2-E_2^2$. The boundaries of integration for $P_Q(T_1=1)$ and $P_V(T_1=\infty)$ are thus identical to the boundaries for U, but with a change of ψ_S. Finally, the PDFs $P_V(T_1=1)$ and $P_Q(T_1=\infty)$ reduce to line integrals, with $E_2=\sqrt{E_1^2-V}$ and $E_2=\sqrt{E_1^2-Q}$, respectively.

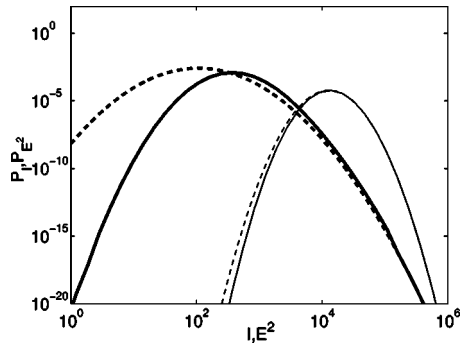

FIG. 5. P_{E^2}, P_I for orthonormal modes in Table I. Thick and thin dashed curves correspond to the field PDFs $P_{E_1^2}$ and $P_{E_2^2}$, while the thick and thin solid curves correspond to P_I for the convolution of $P_{E_1^2}$ with $P_{E_1^2}$ [cases (i), (iii), and (v) in Table I] and $P_{E_1^2}$ with $P_{E_2^2}$ [cases (ii), (iv), and (vi) in Table I], respectively.

B. Distribution functions for the Stokes parameters and the degrees of polarization

Figure 5 shows the distributions $P_{E_1^2}$, $P_{E_2^2}$, and P_I for the cases shown in Table I. The field strength convolution calculations agree with those of Cairns *et al.* [23] for two similar distributions (Fig. 6 in that work). The dominance of the resultant PDF of $I=E_1^2+E_2^2$ by one field population is expected given the distributions used, for which $\langle E_1^2\rangle\ll\langle E_2^2\rangle$, and so $I\simeq E_2^2$.

Figure 6 shows P_U for all cases in Table I. For orthonormal modes, the expression for U is independent of $|T|$, so the PDF is independent of the mode polarization. The two weak peaks in the PDF [labeled $\max(P_U)$ in the figure] correspond to the lower singular boundary sweeping through statistically significant regions of E space, as shown in Fig. 7. Physically, this corresponds to the superposition of wave packets with

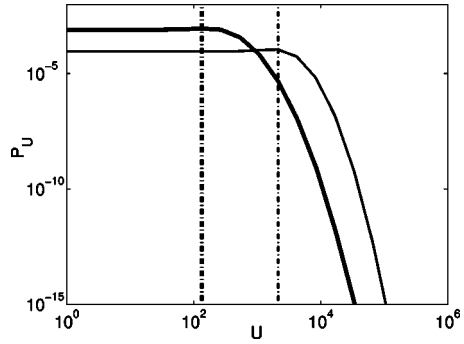

FIG. 6. P_U for orthonormal modes $T_1=0.5$, $T_2=-2$. Solid and dashed curves describe $P_U(U>0)$ and $P_U(U<0)$, respectively, for case (i) (thick) and case (ii) (thin) of Table I.

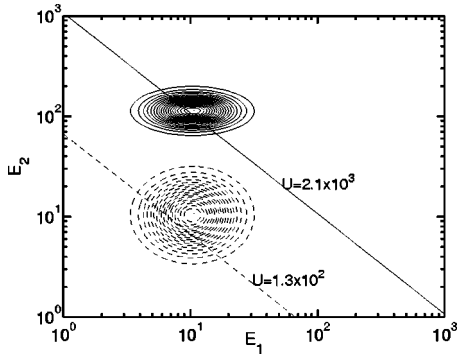

FIG. 7. Log-log contour plot of the product $P_{E1}^2 P_{E2}^2$ for wave modes with a dominant field distribution (solid) and equal field strength distributions (dashed). Overlaid are the lower singular boundaries of integration for P_U at the peaks in P_U.

$E_1 \simeq \langle E_1 \rangle$, $E_2 \simeq \langle E_2 \rangle$ with phase difference $\pi/2$. The nonzero limit for $P_U(0)$ occurs because the region of integration, $\int dE_1^2 dE_2^2$ converges to a fixed nonzero value as $U \to 0$.

Figure 8 shows P_V for the three different wave polarizations [Fig. 8(a) is elliptic, Fig. 8(b) circular, and Fig. 8(c) linear] for the two different field strength PDF combinations. For cases in which the component field strength PDFs are equal and/or the polarization linear, P_V is symmetric about $V=0$. In Figs. 8(a) and 8(b), the peak for $V<0$ lies near the mean of the superposed wave populations $\langle V \rangle = \langle V_1 \rangle + \langle V_2 \rangle$, as denoted by the markers. In Fig. 8(c), which corresponds to linear polarization, the peaks of V lie near but not at $V=0$. For linearly polarized modes, the expression for V is related to U through $U/V = \tan \psi$, so the boundaries for V are the same as those for U, but with a phase shift in ψ. The peaks in V thus correspond to the lower singular boundaries ($\psi = \pi/2$) sweeping through statistically significant regions of E space, as in Fig. 7. Finally, in all examples, the nonzero limit for $P_V(0)$ occurs for the same reason as $P_U(0)=0$: convergence of the boundaries in E space to enclose a fixed nonzero region.

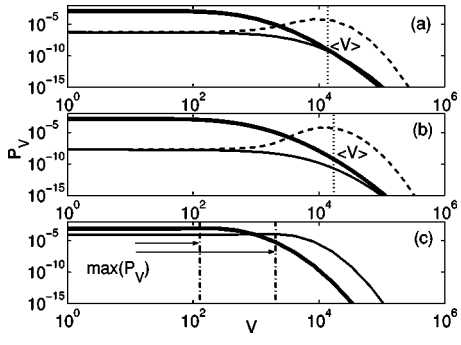

FIG. 8. P_V for orthonormal modes of (a) elliptic, (b) circular, and (c) linear polarizations. Thick and thin curves describe the superposition of two modes with equal field strength distributions [cases (ii), (iv), and (vi) of Table I], and two modes where one mode has a dominant field strength distribution [cases (ii), (iv), and (vi) of Table I], respectively. Solid and dashed curves describe $P_V(V>0)$ and $P_V(V<0)$, respectively. The dash-dotted lines show the positions of peak P_V.

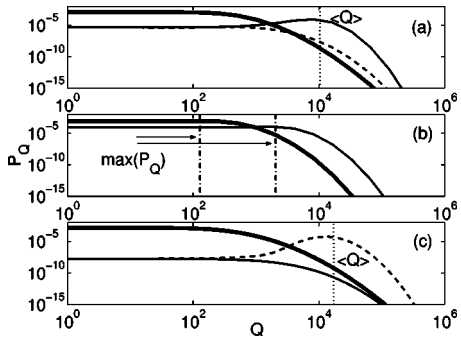

FIG. 9. P_Q for orthonormal modes of (a) elliptic, (b) circular, and (c) linear polarizations. Thick and thin curves describe the superposition of two modes with equal field strength distributions [cases (ii), (iv), and (vi) of Table I], and two modes where one mode has a dominant field strength distribution [cases (ii), (iv), and (vi) of Table I], respectively. Solid and dashed curves describe $P_Q(Q>0)$ and $P_Q(Q<0)$, respectively. The dash-dotted lines show positions of peak P_Q.

Figure 9 shows P_Q. The features for the three different polarization cases can be understood by noting that the expressions for V and Q are related by the interchange mapping of Eq. (76). For case (i), the $V<0$ and $Q>0$ PDFs are qualitatively identical, with the slight shift in $\langle Q \rangle$ accounted for by the change in T_1 in the mapping of Eq. (76). For linearly and circularly polarized modes the relationship between Q and V is transparent through the mapping $Q(T_1=1) = -V(T_1=\infty)$; $Q(T_1=\infty) = V(T_1=1)$. This explains why Figs. 8(b), 9(c), 8(c), and 9(b) are identical.

Figures 10, 12, and 13 plot the PDFs for the degree of circular and linear polarization for the three different types of wave polarizations. For case (i) of Table I, shown in Fig. 10, the degree of circular polarization is dominated by the stronger field, with mean $\langle v \rangle = -0.8$. There is also, however, a split in the peak of the PDF, with peaks slightly below the mean ($v=-0.85$) and above it ($v=-0.75$)). Analytically, these occur because the upper singular boundary of integration sweeps through statistically significant regions of E space as v is perturbed from the mean of the dominant mode $\langle v_2 \rangle = -0.8$. Physically, the two peaks correspond to the superposition of initially [at $t=0$, where all phases in Eq. (3) have

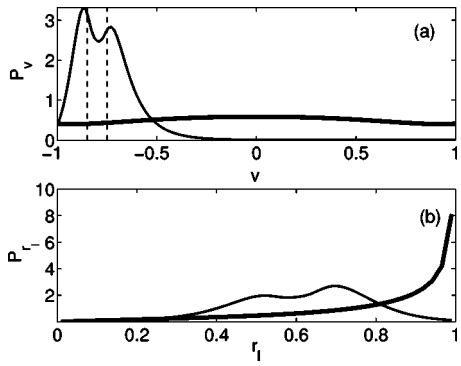

FIG. 10. Plot of (a) P_v and (b) P_{r_l} for elliptically polarized modes $T_1=0.5$, $T_2=-2$. Thick and thin solid lines describe PDFs for cases (i) and (ii) of Table I, respectively.

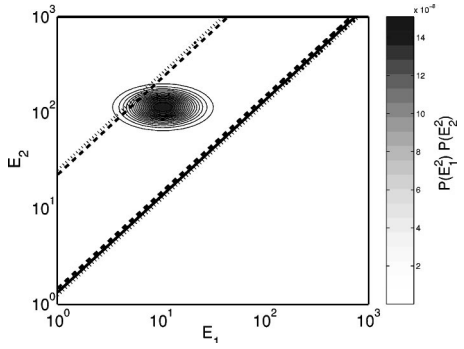

FIG. 11. Log-log contour plot of $P_{E1}^2 P_{E2}^2$. Overlaid are the singular boundaries of integration for $v=-0.8$ (solid), $v=-0.75$ (dotted), and $v=-0.85$ (dashed). The upper boundary for $v=-0.8$ is at infinity.

been accounted for] parallel and antiparallel vectors near the mean field strengths of each wave population. This is shown in Fig. 11, where the boundaries of integration are overplotted on a contour plot of the numerator of the integrand, $P_{E1}^2 P_{E2}^2$. For $v=-0.85$ the upper boundary is at $\psi=0$, corresponding to the addition of two initially parallel vectors, while the upper boundary for $v=-0.75$ is at $\psi=\pi$, corresponding to the addition of two initially antiparallel vectors. In both cases the upper boundaries pass near the peak in the distribution functions. At $v=-0.8$ (where $\overline{\beta}=0$), corresponding to the circular polarization of the dominant mode, the lower and upper boundaries lie on $E_1=0$ and $E_2=-E_1\overline{\alpha}/\overline{\gamma}$.

The two peaks in the PDF for the degree of linear polarization in Fig. 10(b) correspond to the two peaks in the PDF for the degree of circular polarization Fig. 10(a). For the superposition of modes with equal field strength PDFs, P_v is symmetric about $v=0$, with a peak at $v=0$. This corresponds to a PDF biased toward $r_l=1$.

In Fig. 12 PDFs for the degree of circular and linear polarization are shown for circularly polarized wave modes. When combining wave populations of unequal field strength [case (iii) of Table I], the PDF for the degrees of polarization are skewed toward the dominant field, thus explaining the peak in P_v near $v=-1$. The superposition of orthonormal circularly polarized waves of equal field strength PDFs

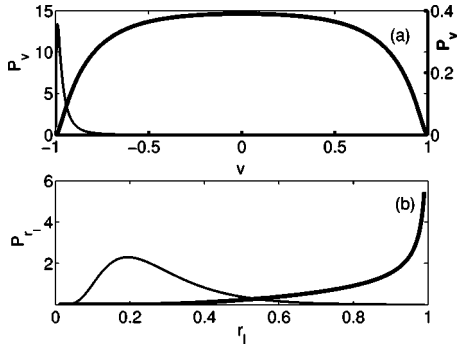

FIG. 12. Plot of (a) P_v and (b) P_{r_l} for circularly polarized modes $T_1=1$, $T_2=-1$. Thick and thin solid lines describe PDFs for cases (iii) and (iv) of Table I, respectively. The vertical scale for the thick curve in (a) is on the right-hand vertical axis.

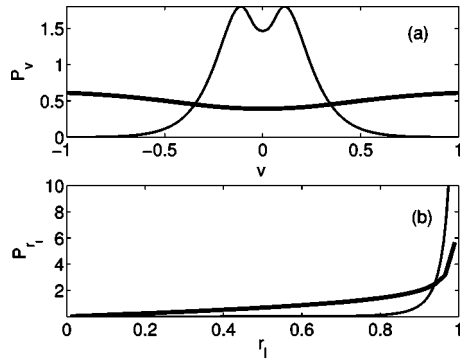

FIG. 13. Plot of (a) P_v and (b) P_{r_l} for linearly polarized modes $T_1=\infty$, $T_2=0$. Thick and thin solid lines describe PDFs for cases (v) and (vi) of Table I, respectively.

yields P_v symmetric about $v=0$ and with peak at $v=0$, corresponding to a peak in P_{r_l} at $r_l=1$.

Finally, Fig. 13 plots the degrees of circular polarization for linearly polarized modes. As for case (i), shown in Fig. 10, the PDF of the central peak at $v=0$ is dominated by the stronger field. The two peaks either side of $v=0$ result from the same phenomenon described for elliptically polarized modes.

V. CONCLUSIONS

In this work we have described the polarization statistics of the superposition of multiple wave populations. Each wave population was considered to be a coherent mode with fixed axial ratio and polarization angle, and the electric field strength and phase were taken to be random variables with arbitrary distributions. Our analysis builds upon the treatment of Cairns *et al.* [23], in which two wave vectors with fixed polarization angle but random phase difference were superposed. Using this representation, integral expressions were developed for the PDFs P_S of the Stokes parameters S (a label for I, U, Q, and V), as well as the degrees of linear and circular polarization of the superposed wave populations. For two wave populations, it was shown that the integral for each Stokes PDF P_S contains a square-root singularity in electric field space. Finally, predictions for the Stokes parameters and degrees of polarization were computed for three different component wave polarizations (elliptic, circular, and linear), and two different lognormal field strength PDFs (a dominant mode and equal field strength PDFs).

The present work differs from earlier treatments (e.g., Hurwitz [7], Barakat [8,9], and Eliyahu [10]), which superpose E_x and E_y correlated Gaussian fields, where each field has a random but uniformly distributed phase. Their analysis is equivalent to our treatment in the special case that the plasma modes are linearly polarized, the phases are uniformly distributed, the electric fields have a Gaussian distribution, and the average value of V is zero for the superposed waves.

The main results of the present work can be summarized as follows.

(1) The superposition of two orthonormal modes leads to the superposition of individual intensities for the total inten-

sity $I=E_1^2+E_2^2$, and therefore a convolution of $P_{E_1^2}$ and $P_{E_2^2}$ for P_I.

(2) For orthonormal mode pairs, a simple mapping was found to relate the expressions for Q and V.

(3) For orthonormal modes, as U, Q, and V approach zero, the PDFs P_U P_Q, and P_V converge to nonzero values, corresponding to convergence of the boundaries of integration in E space to enclose a nonzero region.

(4) For wave populations in which there is a dominant field, the PDF for the Stokes parameters in statistically significant regions is dominated by the dominant wave population. The mean $\langle S\rangle$ is confirmed to be equal to the sum of the mean of the Stokes parameters of the n individual wave populations. That is, $\langle S\rangle=\langle S_1\rangle+\langle S_2\rangle+\cdots+\langle S_n\rangle$.

(5) Except for circularly polarized light, the addition of a weaker field leads to a double peak of the PDF of the degree of circular polarization. Physically, the two peaks correspond to the superposition of initially parallel and antiparallel vectors near the peak field strength of each wave population. For circularly polarized light, the effect of the weaker population is to shift the PDF peak for P_v away from $|v|=1$, and move the PDF peak for P_{rl} away from $|r_l|=0$.

(6) The superposition of wave vectors with equal field strength PDFs gives rise to PDFs for U, Q, and V symmetric about $U=0$, $Q=0$, and $V=0$, with expectation values of zero, but peaks at nonzero U, Q, and V. Physically, these peaks correspond to the superposition of vectors near peak field strength, and initially $\pi/2$ out of phase.

(7) The degree of circular polarization of the superposed mode can exceed in magnitude the degree of circular polarization of either component mode. In this case, there exist four sets of orthonormal mode pairs, each with the same phase difference and one common field strength, which superpose to form a wave with the same degree of circular polarization.

(8) Comparison between the predictions for the degree of linear and circular polarization (e.g., Figs. 10 and 13) and the polarization properties of the component waves suggests that the interpretation of polarity resolved data (e.g., from pulsars) is not trivial. In part, the reason is that the multiple peaks predicted are not at the same locations as for the component distributions. Even when the field strength of one mode is fixed, however, there are multiple ways to combine mode pairs with the same phase difference to obtain the same degree of circular polarization. That is, the problem is degenerate in the phase difference and fixed field strength of one mode. Investigating such subtle effects in real data is therefore challenging, and of considerable interest.

ACKNOWLEDGMENTS

This work was supported by the Australian Research Council and a University of Sydney Sesqui Grant.

[1] P. Bak, C. Tang, and K. Wiesenfeld, Phys. Rev. Lett. **59**, 381 (1987).
[2] B. J. Rickett, Annu. Rev. Astron. Astrophys. **28**, 561 (1990).
[3] P. A. Robinson, Phys. Rev. B **55**, 12 175 (1997).
[4] P. A. Robinson, Phys. Plasmas **2**, 1466 (1995).
[5] D. B. Melrose and R. C. McPhedran, *Electromagnetic Processes in Dispersive Media* (Cambridge University Press, Sydney, 1991).
[6] J. D. Jackson, *Classical Electrodynamics*, 3rd ed. (John Wiley and Sons, New York, 1998).
[7] H. Hurwitz, J. Opt. Soc. Am. **35**, 525 (1945).
[8] R. Barakat, Opt. Acta **32**, 295 (1985).
[9] R. Barakat, J. Opt. Soc. Am. A **4**, 1256 (1987).
[10] D. Eliyahu, Phys. Rev. E **50**, 2381 (1994).
[11] I. H. Cairns and P. A. Robinson, Phys. Rev. Lett. **82**, 3066 (1999).
[12] I. H. Cairns, P. A. Robinson, and R. R. Anderson, Geophys. Res. Lett. **27**, 61 (2000).
[13] C. R. Boshuizen, I. H. Cairns, and P. A. Robinson, Geophys. Res. Lett. **28**, 3569 (2001).
[14] I. H. Cairns and J. D. Menietti, J. Geophys. Res., [Atmos.] **106**, 515 (2001).
[15] I. H. Cairns and K. A. Grubits, Phys. Rev. E **64**, 056408 (2001).
[16] P. A. Robinson, I. H. Cairns, and D. A. Gurnett, Astrophys. J. **407**, 790 (1993).
[17] I. H. Cairns, S. Johnston, and P. Das, Astrophys. J. **563**, L65 (2001).
[18] A. Bershadskii and K. R. Sreenivasan, Eur. Phys. J. B **35**, 513 (2003).
[19] J. Hanasz, M. Panchenko, H. de Feraudy, R. Schreiber, and M. M. Mogilevsky, J. Geophys. Res., [Atmos.] **108**, 1408 (2003).
[20] B. A. Carreras *et al.*, Phys. Plasmas **5**, 3632 (1998).
[21] I. H. Cairns and P. A. Robinson, Astrophys. J. **509**, 471 (1998).
[22] P. A. Robinson, Rev. Mod. Phys. **69**, 507 (1997).
[23] I. H. Cairns, P. A. Robinson, and P. Das, Phys. Rev. E **66**, 066614 (2002).
[24] H. C. Van de Hulst, *Light Scattering by Small Particles* (John Wiley and Sons, New York, 1957).
[25] C. Brosseau, *Fundamentals of Polarized Light: A Statistical Optics Approach* (Wiley, New York, 1998).
[26] W. H. Press, S. A. Teukolsky, W. T. Vetterling, and B. P. Flannery, *Numerical Recipes in Fortran 77 and Fortran 90*, 2nd ed. (University of Cambridge Press, Cambridge, England, 1997).